

Electronic and phononic properties of the chalcopyrite CuGaS₂

A.H. Romero,¹ M. Cardona,² R. K. Kremer,^{2,*} R. Lauck,² G. Siegle,² C. Hoch,² A. Muñoz,³ and A. Schindler⁴

¹CINVESTAV, Departamento de Materiales, Unidad Querétaro, Querétaro, 76230, Mexico

²Max-Planck-Institut für Festkörperforschung, Heisenbergstrasse 1, D-70569 Stuttgart, Germany

³MALTA Consolider Team, Departamento de Física Fundamental II,

and Instituto de Materiales y Nanotecnología, Universidad de La Laguna, La Laguna 38205, Tenerife, Spain

⁴NETZSCH-Gerätebau GmbH, Wittelsbacherstr. 42, D-95100 Selb, Germany

(Dated: October 15, 2018)

The availability of *ab initio* electronic calculations and the concomitant techniques for deriving the corresponding lattice dynamics have been profusely used for calculating thermodynamic and vibrational properties of semiconductors, as well as their dependence on isotopic masses. The latter have been compared with experimental data for elemental and binary semiconductors with different isotopic compositions. Here we present theoretical and experimental data for several vibronic and thermodynamic properties of CuGaS₂, a canonical ternary semiconductor of the chalcopyrite family. Among these properties are the lattice parameters, the phonon dispersion relations and densities of states (projected on the Cu, Ga, and S constituents), the specific heat and the volume thermal expansion coefficient. The calculations were performed with the ABINIT and VASP codes within the LDA approximation for exchange and correlation and the results are compared with data obtained on samples with the natural isotope composition for Cu, Ga and S, as well as for isotope enriched samples.

PACS numbers: 63.20.-e, 63.20.dk, 63.20.D-, 68.35.bg, 65.40.Ba, 71.55.Gs, 71.70.Ej

I. INTRODUCTION

The availability of *ab initio* electronic calculations and the concomitant techniques for deriving the corresponding lattice dynamics have been profusely used in the past decade for calculating thermodynamic and vibrational properties of semiconductors, as well as their dependence on isotopic masses. The latter have been compared with experimental data for elemental and binary semiconductors with different isotopic compositions.¹⁻³ Here we present theoretical and experimental data for several vibronic and thermodynamic properties of a canonical ternary semiconductor of the chalcopyrite family: CuGaS₂. Two main groups of chalcopyrites are usually considered, one, denoted as I-III-VI₂, derived from the II-VI compounds with zincblende structure, the other, II-IV-V₂, derived from the III-V zincblende compounds. Examples of the first group are CuGaS₂ and AgGaS₂, whereas the second type is represented, for example, by ZnGeAs₂. The chalcopyrite structure has the space group $I\bar{4}2d$ and the class $\bar{4}2m$ with two formula units per primitive cell and a longitudinal distortion along the *c*-axis which converts the tetrahedral primitive cell (PC) into a tetragonal one. The lattice constants of the tetragonal PC are $a = b$ (along *x* and *y*) and *c* (along *z*).⁴ The regular tetrahedra with the anion at the center and the cations at the vertices are distorted because, e.g., of the different lengths of the I-II and the III-II bonds. The anion distortion is usually chosen to be along the *x* direction and equal to $u - 1/4$, $u = 1/4$ corresponds to no tetrahedral distortion. In this article we discuss lattice parameters and vibrational properties of some I-III-VI₂ chalcopyrites (I = Cu, Ag). The motivation for this choice (as opposed to the II-VI-V₂ materials) is that

the copper and silver chalcopyrites have received considerable attention for the production of photovoltaic cells. Their energy gaps cover the range 1 - 3.5 eV, i.e., most of the frequency of the solar spectrum. From the fundamental point of view, these materials have the property that the 3*d* core electrons of Cu and the 4*d* of Ag overlap (and thus hybridize) with the top of their valence bands, and thus giving rise to a number of interesting anomalies involving negative spin orbit splittings (-0.016 eV for CuGaS₂, (Ref. 5) and nonmonotonic behavior of the energy gap versus temperature.⁶

In this article we focus on the chalcopyrite CuGaS₂. These sulfides, CuInS₂ and the corresponding selenides are being considered, together with their alloys, as efficient photovoltaic materials. From the fundamental point of view CuGaS₂ has received less attention than the other related chalcopyrites, a reason why here we concentrate on the physical properties of this material. CuGaS₂ was first synthesized by Hahn *et al.*⁷ They also determined by X-ray diffraction the crystal structure and the lattice parameters $a = b$, *c*, and *u* of this and 19 other related chalcopyrite compounds. Many of these parameters agree reasonably well with those determined experimentally up to date and also with recent *ab initio* calculations. CuGaS₂ was first found as a mineral (gallite) in Namibia and in the Kongo.^{8,9}

CuGaS₂ crystallizes with the chalcopyrite structure which is closely related to that of zincblende with a slight distortion resulting from the tetrahedral bonding of the latter.⁷

II. THEORETICAL DETAILS

The calculations reported here concern the lattice parameters of CuGaS_2 , the Raman, ir active, and silent $k = 0$ phonons, their Grüneisen parameters and the phonon dispersion relations, the densities of phonon states (DOS) (including the projections on the vibrations of the 3 component atoms), and the optically active densities of two-phonon states. In addition, we present *ab initio* calculations of the elastic constants and the bulk moduli B_0 and B_0' . Because of the large number of phonon at $k = 0$ (24) we surmised that for a calculation of the volume expansion coefficient vs. T a BZ sampling using only the 24 Grüneisen parameters of these phonons (at $k \approx 0$) would yield a reasonable approximation to the scarce experimental results available. This conjecture turned out to be correct. Finally, we used the calculated phonon density of states (PDOS) to evaluate the specific heat at constant volume (and the expansion coefficient to evaluate the measured constant pressure counterpart). These calculations were performed with the natural isotopic abundance of the constituents of CuGaS_2 and also for crystals composed of isotopically pure atoms.

The calculations were based on *ab initio* electronic band structure determinations using density functional theory with either the ABINIT or the VASP code.^{10–13} In the ABINIT calculation, normalized pseudo potentials were generated by using the Fritz Haber Institute code with a valence electron configuration of $3d^{10} 4s^1$ for Cu, $3d^{10} 4s^2 4p^1$ for Ga and $3s^2 3p^4$ for S.¹⁴ The wave function was expanded in plane wave up to an energy cutoff of 40 Ha and the Brillouin zone was sampled by using the Monkhorst-Pack method with a $6 \times 6 \times 6$ \mathbf{k} -point grid. While most electronic calculations were performed without spin-orbit (SO) interaction, in order to reveal possible effects of this interaction on the lattice properties as well as the negative sign of the SO splitting at the top of the valence band, a few band structure calculations with the VASP code including SO interaction were also performed. The effects of this interaction on the lattice parameters and dynamics was found to be insignificant. We display in Fig. 1 the electronic band structure calculated with the VASP code using the LDA exchange-correlation potential without SO interaction. The details of the *ab initio* electronic band structure calculations have been given in Ref. 15.

This band structure is similar to those reported recently by Soni *et al.* and Brik using a GGA exchange-correlation potential.^{18,19} Notice that in our case and that of Soni *et al.* the direct gap (1 - 2 eV) is considerably smaller than the experimental one (2.43 eV), a rather general property of LDA calculations sometimes referred to as the "gap problem".¹⁶ Brik brought the calculated gap to agree with the experimental one by using the so-called 'scissors operator'.¹⁹

An interesting feature of the band structures of Fig. 1 and Ref. 18 is the fact that the bands which correspond to the $3d$ electrons of the copper overlap with the $2p$

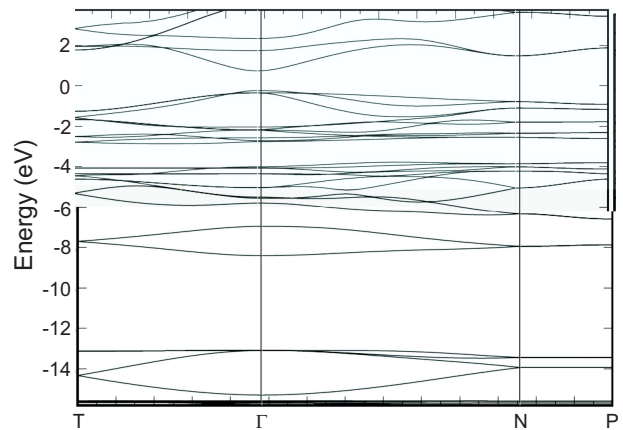


FIG. 1: Electronic band structure of CuGaS_2 calculated with the VASP code using the LDA exchange-correlation potential without SO interaction. The four lowest bands involve mainly $3s$ electrons of S. The bands between 0 and -8 eV correspond to twenty $3d$ electrons of Cu and twenty four $3p$ of S. Notice that the calculated energy gap (1.1 eV) is much smaller than the experimental one (2.4 eV, Ref. 4), reflecting the so-called "gap-problem".¹⁶ The notation of the special points in the Brillouin zone (Γ - Γ - N - P) is identical to that of Ref. 17.

bands of sulfur. This peculiarity results in a negative SO splitting at the top of the valence bands (-0.016 eV) (Ref. 20), an anomalous sign also observed in CuCl (Ref. 21), ZnO (Ref. 22), and $\beta\text{-HgS}$ (Ref. 22,23). Here we shall no longer discuss electronic properties of chalcopyrites and concentrate on the lattice parameters, phonons and thermodynamic properties.

The reader may wonder why we use two different DFT codes. The reason is that we are familiar with both codes and, while we know that they lead to similar results in the case of monoatomic and binary crystals, it is not obvious that they also will do so for more complicated structures. This was shown to be so in the case of cinnabar ($\alpha\text{-HgS}^{23}$), with three atoms per PC. Here we examine chalcopyrites, with 8 atoms per PC.

The wave function representation for the two codes is different as well as the methodology e. g. to calculate the phonon vibrational spectra. Therefore, the use of both codes is complementary. In some cases, the ABINIT code is more computationally demanding but the precision can be increased. Therefore, for some properties, such as the phonon spectra, we have employed the ABINIT implementation where density functional perturbation theory was used.^{24,25}

III. EXPERIMENTAL DETAILS

The CuGaS_2 crystals investigated here were grown by a vapor phase transport technique using iodine as transport agent. The isotopically nearly pure (99.5% ^{34}S , 99.9% ^{63}Cu and 99.6% ^{72}Ga) elements were purchased from Trace Science International, Ontario, Canada.

For the single crystal X-ray structure determination CuGaS₂ crystals were selected under the polarization microscope for crystallographic investigations. As many of the crystals showed twinning according to $\bar{1}$, with $\mathbf{1}$ being the identity operation, a small cuboid fraction ($0.24 \times 0.20 \times 0.14 \text{ mm}^3$) of a yellow transparent crystal was oriented on a four-circle diffractometer using graphite-monochromatized Ag-K α radiation (CAD 4, Enraf Nonius, Delft, The Netherlands). The lattice parameters of the tetragonal lattice (space group $I\bar{4}2d$, No. 122) were refined from 25 centered high-indexed reflections to $a = 5.3512(6)$ and $c = 10.478(3)$ Å. Bragg intensities in three octants of the Ewald sphere ($-9 \leq h, k \leq 9, -18 \leq l \leq 18, 3.4^\circ \leq \vartheta \leq 29.9^\circ$, $R_{int} = 0.0648$ after merging) were collected in the ω - 2ϑ data acquisition mode and corrected for Lorentz, polarization and absorption effects. The structure refinement was performed with full matrix least-squares cycles on F^2 ($R1 = 0.0472$ for $I \geq 2 \sigma I$ and 0.0832 for all I , $wR2 = 0.1178$ for $I \geq 2 \sigma I$ and 0.1350 for all).²⁶

Temperature dependent lattice parameters and the thermal expansion coefficients were determined by powder X-ray diffraction ($\lambda = 1.54$ Å) on crushed crystals grown from elements with the natural isotopic abundance.

The heat capacities were measured on samples of typically ~ 20 mg between 2 and 280 K with a physical property measurement system (Quantum Design, San Diego, CA) as described in detail in Ref. 28. Between room temperature and 1100 K the heat capacities of a ~ 100 mg polycrystalline sample were determined with a DSC 404 F1 Pegasus differential scanning calorimeter (heating rate 20 K/min) with the sample kept in an argon atmosphere.²⁷ Up to 1100 K a reduction of the sample mass was not observed.

IV. RESULTS AND DISCUSSION

A. Crystal Structure

The available structural parameters of CuGaS₂ exhibit considerable dispersion, especially the x positional parameter of the S atoms which is very close to $1/4$ (in the forthcoming called u) has so far been determined with limited reliability and found to be larger than $1/4$. Additionally, u has been found to vary non-monotonically from CuAlS₂, via CuGaS₂ to CuInS₂.⁴ In order to increase the accuracy of u we redetermined the crystal structure of CuGaS₂ using high-quality single crystals and up-to-date X-ray diffraction techniques which allow us to decrease the experimental error in u by a factor of ~ 7 . Table IV A summarizes the results of our crystal structure redetermination.

The positional parameter u is clearly smaller than $1/4$ ($\sim -2.5\%$) and decreases monotonically throughout the series CuAlS₂ - CuGaS₂ - CuInS₂. Table II summarizes the experimental and calculated structural parameters of

CuXS₂ (X = Al, Ga, In) as obtained from our calculations and as available in the literature.

Since the available calculations did not include SO splitting we performed, for comparison, calculations with SO splitting. They are displayed in Table III together with a VASP-NOSO calculation carried out by Chen *et al.*³⁰ using a GGA DFT for the exchange-correlation hamiltonian.

B. Elastic Properties

The ABINIT code used for our calculations provides also the stiffness constants, C_{ij} ,³¹ six independent ones in the case of the chalcopyrites (Table IV).

We have not been able to retrieve experimental values for these from the literature. In Table IV we display for comparison data for CuGaSe₂ and AgGaS₂. For the latter experimental data are also quoted. We have also included bulk moduli, B_0 , and their pressure derivative, B_0' , for all three compounds. Except for B_0' , all elastic parameters undergo a monotonic decrease through the series CuGaS₂, CuGaSe₂ to AgGaS₂, which is likely to be related to the corresponding increase of the lattice parameters.

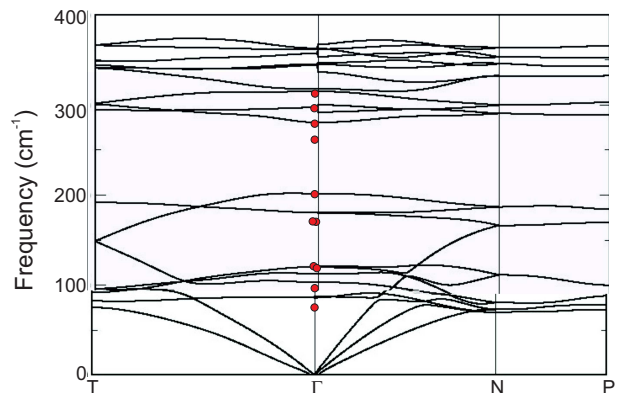


FIG. 2: (color online) Phonon dispersion relations of CuGaS₂ as calculated with the ABINIT-LDA code. The notation of the special points in the Brillouin zone (T - Γ - N - P) is identical to that of Ref. 17. The (red) dots represent some of the available experimental frequencies (see Table V).

The calculated phonon dispersion relations are shown in Fig. 2 in the reduced Brillouin zone. The Γ - T direction corresponds to $[001]$ whereas Γ - N corresponds to $[110]$.¹⁷ For comparison, we have added a few points obtained from Raman and infrared spectroscopy measurements given in more detail in Table V where they are also compared with our *ab initio* calculations and those of Akdoğan *et al.*^{37,38}

Figure 3 displays the phonon densities of states corresponding to the motion of the three constituent atoms calculated from the dispersion relations shown in Fig. 2. As expected, the low-frequency band $0 - 100 \text{ cm}^{-1}$ corresponds mainly to Cu and Ga vibrations whereas the S-

TABLE I: Summarized results of the crystal structure determination ($T = 293(2)$ K) of CuGaS_2 (space group $\bar{I}42d$, No. 122). Standard deviations of the last digit are given in parentheses. The lattice parameters were determined to be $a = 5.3512(6)$ Å, $c = 10.478(3)$ Å resulting in a unit cell volume of $300.03(9)$ Å³ which contains 4 formula units ($Z = 4$). Further experimental details are deposited under the no. CSD-422615 at the Fachinformationszentrum Karlsruhe.²⁶

Fractional atomic coordinates and equivalent isotropic displacement parameters (Å ²)						
Atom	Wyckoff-Nr.	x	y	z	U_{equiv}	
Ga	4a	0	0	0	0.0078(4)	
Cu	4b	0	0	$\frac{1}{2}$	0.0159(4)	
S	8d	0.2437(5)	$\frac{1}{4}$	$\frac{1}{8}$	0.0085(4)	
Anisotropic displacement parameters U_{ij} (Å ²)						
Atom	U_{11}	U_{22}	U_{33}	U_{12}	U_{13}	U_{23}
Ga	0.0080(4)	0.0080(4)	0.0076(5)	0	0	0
Cu	0.0155(5)	0.0155(5)	0.0165(6)	0	0	0
S	0.0113(11)	0.0051(10)	0.0092(6)	0	0	-0.0016(5)

like contributions are mainly above the ~ 280 cm⁻¹-gap. we note that there are also some S-like contributions below ~ 120 cm⁻¹ originating from Cu - S vibrations. The partial densities of states are e.g. useful for calculating the effect of isotope disorder on the phonon linewidths.³⁹

We have not found in the literature second-order Raman spectra of CuGaS_2 which would correspond to the sum and difference spectra of Fig.2. Nevertheless, it is possible to establish a correspondence between the calculated two-phonon Raman spectra of CuGaS_2 and (Fig.3) and the measured ones of β -ZnS shown in Fig. 1 of Ref. 40. We present here the calculated sum and difference densities of states of CuGaS_2 in the hope that they will help in interpreting measured spectra when they become available for the CuGaS_2 or other chalcopyrite compounds.

Table V also lists the calculated and experimental Grüneisen parameters of Γ -point phonons. As usual, most of the the Grüneisen parameters are positive except some at the lowest frequencies.

The effect of lattice vibrations on the volume $V_0(T)$ of a (cubic) crystal can be expressed in terms of the mode Grüneisen parameters γ_{qj} and the mode frequency as

$$\frac{\Delta V_0(T)}{V_0} = \frac{\hbar}{B_0 V} \sum_{qj} \gamma_{qj} \omega_{qj} [n_B(\omega_{qj}) + \frac{1}{2}], \quad (1)$$

where n_B is the Bose-Einstein factor

TABLE II: Comparison of the results of VASP-NOSO-LDA calculations performed for the three isostructural compounds CuXS_2 ($X = \text{Al, Ga, In}$) with experimental data obtained in this work and in the literature.

parameter	CuAlS_2^a		CuGaS_2		CuInS_2^a	
	VASP	exp	VASP	exp	VASP	exp
$a = b$ (Å)	5.2055	5.326	5.226	5.3512(6)	5.482	5.5221
c (Å)	10.3765	10.436	10.380	10.478(3)	10.9301	11.1043
u	0.2505	0.271	0.2450	0.2437(5)	0.21651	0.2145

^a Ref. 29 and average values of references therein.

TABLE III: Lattice parameters, fractional x atomic coordinate of sulphur (u), cell volume and bulk moduli, B_0 and B_0' as obtained from our *ab initio* calculations either with spin-orbit coupling (SO) or without (NOSO).

code	a (Å)	c (Å)	u	V_{cell} (Å ³)	B_0 (GPa)	B_0'
ABINIT-NOSO	5.262	10.45197	0.244	289.4	93.3	4.7
VASP-NOSO-LDA	5.226	10.380	0.2450	283.5	94.3	4.5
VASP-SO-LDA	5.2258	10.3818	0.2450	283.5	91.9	5.1
VASP-NOSO-GGA ^a	5.3700	10.643	0.2491	306.9	85	4.7

^a Ref. 30

TABLE IV: Comparison of the stiffness constants obtained from ABINIT calculations performed for the three isostructural compounds CuGaS_2 , CuGaSe_2 and AgGaS_2 with experimental data obtained in this work and in the literature.

parameter	CuGaS_2		CuGaSe_2		AgGaS_2	
	calc	exp	calc	exp	calc	exp
C_{11} (GPa)	132.23	-	112.2 ^a	-	85.3 ^b	86.5 ^b
C_{12} (GPa)	78.4	-	66.4 ^a	-	52.4 ^b	56.0 ^b
C_{13} (GPa)	79.4	-	68.1 ^a	-	59.9 ^b	59.6 ^b
C_{33} (GPa)	144.1	-	113.2 ^a	-	76.2 ^b	75.1 ^b
C_{44} (GPa)	56.1	-	48.4 ^a	-	32.4 ^b	24.9 ^b
C_{66} (GPa)	56.3	-	48.5 ^a	-	36.1 ^b	31.4 ^b
B_0	96.4	94 ^c , 96 ^d , 97 ^e	83 ^a	102 ^a	60 ^d , 62.3 ^b	72.2 ^b
B_0' (GPa)	4.5	6.3 ^d , 4 ^e	-	-	4.2 ^b	4 ^b

^a Ref. 32

^b Ref. 33: average values of references therein.

^c Ref. 34

^d Ref. 35

^e Ref. 36

$$n_B(\omega_{qj}) = [e^{\hbar\omega_{qj}/k_B T} - 1]^{-1}, \quad (2)$$

and V and B_0 are the volume and the bulk modulus of the crystal, respectively.⁴¹

Because of the large number of phonon bands we surmised that the Grüneisen parameters of the phonons

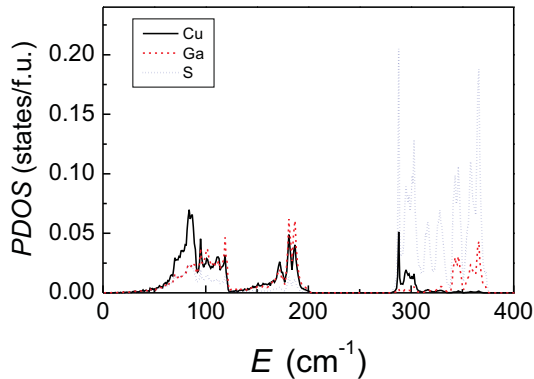


FIG. 3: (color online) Phonon density of states (PDOS) projected on the three constituent atoms. Note the gap between the contributions of (essentially) Cu and Ga (below 200 cm^{-1}) and those above $\sim 280 \text{ cm}^{-1}$ which are essentially S like. There is considerable S like weight below $\sim 120 \text{ cm}^{-1}$. The sum of these partial densities of states has been used to calculate the temperature dependence of heat capacities.

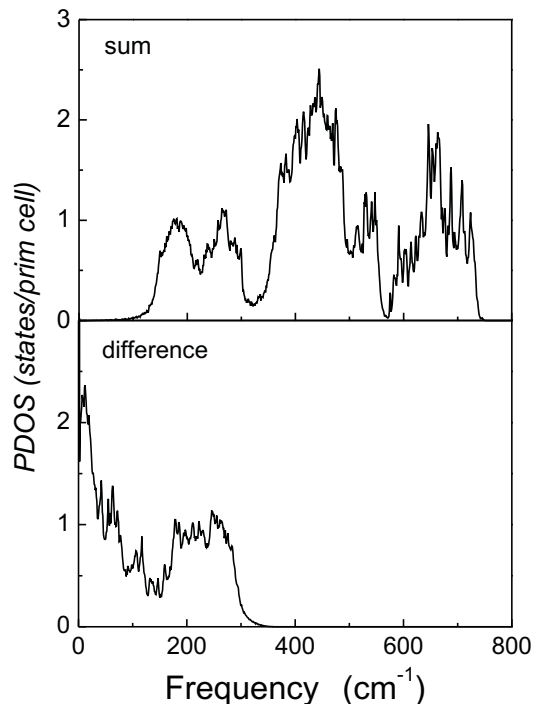


FIG. 4: Sum (upper panel) and difference (lower panel) phonon densities of states of CuGaS_2 as calculated from the dispersion relations shown in Fig. 4.

TABLE V: Calculated and measured phonon frequencies of CuGaS_2 (in cm^{-1}) at the center of the BZ. Also, averaged experimental values reported in about 9 different publications (see Akdoğan *et al.*³⁸, Table 4). The values of the corresponding Grüneisen parameters, γ , calculated by us are also listed and compared with measurements.

irred. reps.	Akdoğan ^a theory	ours ABINIT	ours VASP	exp. ^a	γ ABINIT	γ exp ^b
Γ_1 (A1)	290.0	292	316.8	312	2.04	1.5
Γ_2 (A2)	341.7	314	345.0	silent	1.62	
Γ_2 (A2)	268.7	345	314.0	silent	1.68	
Γ_3 (B1)	329.7	361	361.2	372	1.62	
Γ_3 (B1)	195.7	203	202.7	202	1.31	2.6
Γ_3 (B1)	99.0	114	114.0	117	0.47	
Γ_4^{LO} (B2)	384.7	381.8	361.9	387	1.54	1.5
Γ_4^{LO} (B2)	234.3	292.0	280.2	277	2.04	1.3
Γ_4^{LO} (B2)	99.0	104.7	103.6	95	0.10	
Γ_4^{TO} (B2)	354.0	365.4	361.9	366	1.54	1.4
Γ_4^{TO} (B2)	234.3	280.2	280.2	261	2.07	1.3
Γ_4^{TO} (B2)	98.7	103.6	103.6	95	0.10	2.0
Γ_5^{LO} (E)	367.0	361.2	352.6	387	1.58	1.3
Γ_5^{LO} (E)	327.7	344.9	335.5	350	2.00	
Γ_5^{LO} (E)	240.6	292.1	292.1	277	2.03	1.1
Γ_5^{LO} (E)	162.3	180.7	180.7	169	1.85	1.5
Γ_5^{LO} (E)	116.6	119.4	119.4	148	-1.04	0.8
Γ_5^{LO} (E)	83.3	86.2	86.1	74	-1.04	-0.80
Γ_5^{TO} (E)	345.7	352.6	352.6	365	1.65	1.5
Γ_5^{TO} (E)	313.3	335.5	335.5	331	2.04	1.2
Γ_5^{TO} (E)	236.0	292.1	292.1	292	2.07	1.41
Γ_5^{TO} (E)	161.6	180.7	180.7	162	1.86	0.8
Γ_5^{TO} (E)	116.7	119.4	119.4	115	-0.08	
Γ_5^{TO} (E)	83.3	86.2	86.1	75	-1.04	-0.80

^a Ref. 38

^b Ref. 37

at Γ suffice, to a first approximation, for the evaluation of the volume thermal expansion coefficient, $\alpha_V = (1/V_0) dV_0(T)/dT$, to include in the summation in Eq. (3) the phonons and their Grüneisen parameters at the Γ -point, where V_0 represents the volume of the primitive cell. As usual in semiconductors, negative values of γ_{qj} lead to negative thermal expansion coefficients at low temperatures.⁴² The temperature dependence of V_0 is given by

$$\frac{\Delta V_0(T)}{V_0} = \frac{\hbar}{B_0 V} \sum_j \gamma_j \omega_j \left[n_B(\omega_j) + \frac{1}{2} \right], \quad (3)$$

where ω_j and γ_j are the zone-center phonon frequencies and the Grüneisen parameter, respectively.

The volume thermal expansion coefficient can also be obtained from the variation of the entropy, $S(P, T)$, with pressure via the thermodynamic relationship

$$\alpha_V(T) = -\frac{1}{V} \left(\frac{\partial S(P, T)}{\partial P} \right)_T. \quad (4)$$

We calculated within the ABINIT code the entropy at ambient pressure and for pressures of 0.4 and 1 GPa and took the numerical derivatives. In Fig. 5 we compile these results and the the results of our calculations using the Γ -point phonon frequencies and the mode Grüneisen parameters summarized in Table V (and its temperature derivative), i.e. the volume thermal expansion coefficient, $\alpha_V(T) = (1/V_0) dV(T)/dT$, with literature data by Bodnar *et al.*, Schorr *et al.*, and with our high temperature X-ray data. For comparison we also display the volume thermal expansion coefficient of Reeber and Powell *et al.*.^{43,44,47}

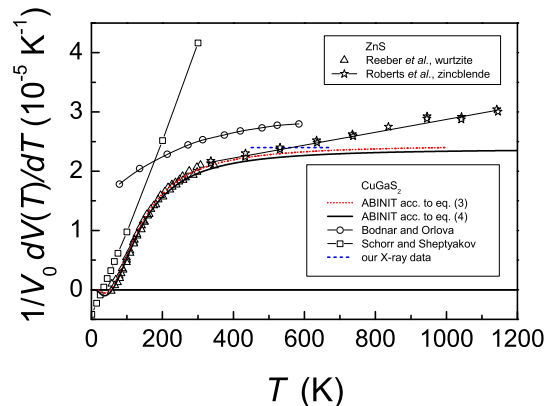


FIG. 5: (color online) (red) dotted line: Temperature dependence of the volume thermal expansion coefficient of CuGaS_2 as obtained from the zone-center Grüneisen parameters γ and frequencies as given in Table V using eq. (3). (black) solid line thermal expansion coefficient from the pressure dependence of the entropy (eq. (4)). Literature data by Reeber *et al.* and Roberts *et al.* and our X-ray results are also given.^{47,48}

The volume thermal expansion coefficients obtained from the Γ -point phonon frequencies and from the pressure-derivative of the entropy are in good agreement, thus justifying the approximation used in eq. (3). The results of our calculations clearly reveal a negative thermal volume expansion coefficient at low temperatures as has been found experimentally by Schorr and Scheptyakov.⁴⁴ However, at high temperatures our calculated data deviate markedly from the experimental findings, they are about 15% lower than the data by Bodnar and Orlova obtained by X-ray diffraction experiments.⁴³ However, there still appears to be some scatter in the experimental data. While Bodnar *et al.* report a room temperature volume thermal expansion coefficient of $24 \times 10^{-6} \text{K}^{-1}$ close to $26.5 \times 10^{-6} \text{K}^{-1}$ obtained by Yamamoto *et al.*, Malsagov *et al.* found a room temperature value of only $19.2 \times 10^{-6} \text{K}^{-1}$, close to the results of our calculations.^{43,45,46} Our calculations also agree rather well with our high-temperature X-ray diffraction data carried out on a polycrystalline sample prepared from the same crystals used for the heat ca-

capacity experiments (see below). The temperature dependence of the volume thermal expansion coefficient for CuGaS_2 is expected to be similar to that of the isobaric and isoelectronic ZnS. This is indeed the case; up to room temperature our calculations coincide remarkably well with volume thermal expansion data for ZnS obtained by Reeber and Powell.⁴⁷ Above room temperature Roberts *et al.* observed a linear increase of the volume thermal expansion coefficient of zincblende ZnS at a rate of $1.16 \times 10^{-8} \text{K}^{-2}$ which is not found in our calculations for CuGaS_2 .⁴⁸ This linear increase of the volume thermal expansion coefficient of wurtzite ZnS and zincblende ZnS has recently also been obtained by *ab initio* calculations.⁴⁹

C. Heat Capacity

The phonon density of states displayed in Fig. 3 allows calculation of the free energy $F(T)$ by using the expression:

$$F(T) = - \int_0^\infty \left(\frac{\hbar\omega}{2} + k_B T \ln[2n_B(\omega)] \right) \rho(\omega) d\omega \quad (5)$$

and of the specific heat at constant volume by taking the second derivative of the free energy

$$C_V = -T \left(\frac{\partial^2 F}{\partial T^2} \right)_V. \quad (6)$$

In Eq. (5), k_B is the Boltzmann constant, n_B the Bose-Einstein factor, and $\rho(\omega)$ the phonon density of states. The high frequency cutoff of the latter defines the upper limit of integration in Eq. (5).

The difference between the calculated heat capacity at constant volume, C_V , and that at constant pressure, C_P , (the quantity that is experimentally obtained) is related to the volume thermal expansion coefficient, α_V , according to

$$C_P(T) - C_V(T) = \alpha_V^2(T) \cdot B \cdot V_{mol} \cdot T, \quad (7)$$

where B_0 is the (isothermal) bulk modulus and V_{mol} the molar volume. With $\alpha_V(T > 300 \text{K}) \approx 2.3 \times 10^{-5} \text{K}^{-1}$ the contribution to the heat capacity from thermal expansion amounts to 0.7 J/molK and 2.3 J/molK at 300 K and 1000 K, respectively.

In the literature heat capacity data for CuGaS_2 are available in the low temperature regime ($13 \text{K} \leq T \leq 38 \text{K}$) and above room temperature up to $\sim 600 \text{K}$.^{50,51} Our data connect these temperature regimes and extend the temperature range up to 1100 K. At low temperature our results are in good agreement with the data of Abrahams and Hsu with improved resolution of the maximum in C_P/T^3 (cf. Fig. 7), at high temperatures they connect well to the data by Neumann *et al.*. In Fig. 6 we display

the heat capacity of CuGaS_2 over a temperature range from 2 K up to 1100 K together with the theoretical results based on the PDOS shown in Fig. 3. To account for the contributions of the thermal expansion, becoming especially noticeable above room temperature, we have used our data of the volume thermal expansion coefficient extended by a linear increase above room temperature of $1.16 \times 10^{-8} \text{K}^{-2}$, identical to that found by Roberts *et al.* for zincblende ZnS .⁴⁸ as displayed in Fig. 5 and used Eq. (7) to calculate C_P .

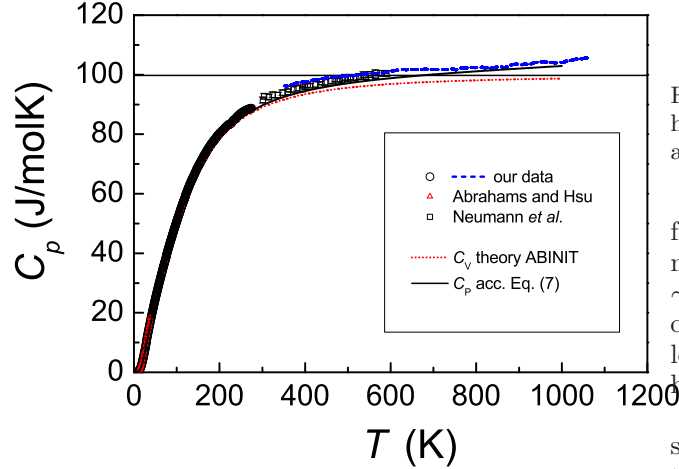


FIG. 6: (color online) Temperature dependence of the molar heat capacity of CuGaS_2 . (o) and (blue) dashed line: our experimental data, (red) dotted line: results of ABINIT calculations of C_V , (black) solid line: C_P according to Eq. (7) using our calculated volume thermal expansion coefficient $\alpha(T)$ displayed in Fig. 5. Above room temperature we have added a linear increase of $\alpha(T)$ which amounted to $1.16 \times 10^{-8} \text{K}^{-2}$, identical to that found by Roberts *et al.* for zincblende ZnS .⁴⁸ Literature data by Abrahams and Hsu and Neumann *et al.* are also displayed.^{50,51} The vertical line indicates the Peti-Dulong value of $12 \times R$, where r is the molar gas constant.

In some of our previous works^{15,52} we have investigated the dependence of C_p/T^3 on the isotopic masses of the constituents of the compounds (up to binary compounds, so far) and compared the experimental data with the theoretical results. For elementary and binary compounds we have also investigated the relationship of the logarithmic derivatives versus temperature and versus the masses of the constituents.⁵²

In all logarithmic derivatives we observe a peak centered at about 20 K. For S there is an additional broad band with its maximum at about ~ 100 K. The maxima in the logarithmic derivatives reflect the structure of the PDOS projected on the corresponding atoms. Clearly, the broad high energy feature visible exclusively for S originates from the PDOS with mainly S character between 280 and 380 cm^{-1} . The ratio of the maximum

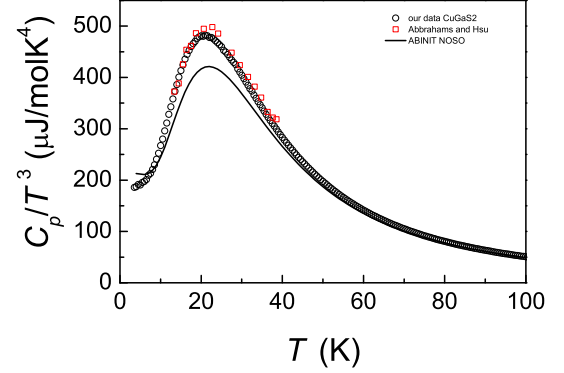


FIG. 7: (color online) Temperature dependence of the molar heat capacity of CuGaS_2 . (o): our experimental data. Literature data by Abrahams and Hsu are also given.⁵⁰

frequency (converted into Kelvin) in the PDOS and the maximum temperature of the logarithmic derivative is ~ 6 , a ratio which has been found in a number of previous investigations.¹⁵ Cu shows the highest feature in the logarithmic derivative at low temperature reflecting the high weight of the Cu projected PDOS at low energies.

We have demonstrated that there is a close relationship of the logarithmic derivatives of the heat capacities with respect to temperature and isotope mass.⁵³ The straightforward extension of the relationship the logarithmic derivatives versus temperature and versus the masses of the isotopes to the ternary compound, CuGaS_2 in our case, is given by

$$\frac{1}{2} \left(3 + \frac{d \ln(C_p/T^3)}{d \ln T} \right) = \frac{d \ln(C_p/T^3)}{d \ln M_{\text{Cu}}} + \frac{d \ln(C_p/T^3)}{d \ln M_{\text{Ga}}} + \frac{d \ln(C_p/T^3)}{d \ln M_{\text{S}}}, \quad (8)$$

where M_{Cu} , M_{Ga} , and M_{S} are the masses of the three constituents, i.e. Cu, Ga, and S, respectively, for CuGaS_2 .

Figure 8 confirms the relationship of the temperature dependence of the logarithmic derivatives with respect to temperature and to the isotope masses established earlier by us is also valid for multinary (in the present case ternary) compounds.

We have demonstrated that for low temperatures, $T \rightarrow 0$, the logarithmic derivatives are related to the ratios of the atomic mass to the molar mass according to⁵²

$$\frac{d \ln C_v/T^3}{d \ln M_{\text{Cu}}} = \frac{3}{2} \frac{M_{\text{Cu}}}{M_{\text{Cu}} + M_{\text{Ga}} + 2M_{\text{S}}} = 0.48 \quad (9)$$

$$\frac{d \ln C_v/T^3}{d \ln M_{\text{Ga}}} = \frac{3}{2} \frac{M_{\text{Ga}}}{M_{\text{Cu}} + M_{\text{Ga}} + 2M_{\text{S}}} = 0.53 \quad (10)$$

$$\frac{d \ln C_v/T^3}{d \ln M_{\text{S}}} = \frac{3}{2} \frac{2M_{\text{S}}}{M_{\text{Cu}} + M_{\text{Ga}} + 2M_{\text{S}}} = 0.49. \quad (11)$$

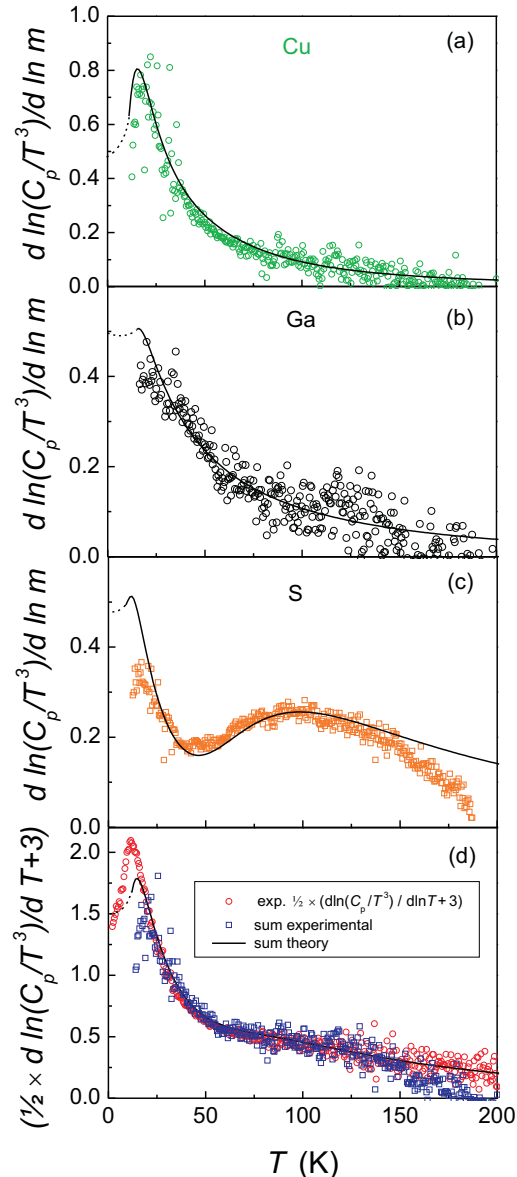


FIG. 8: (color online)(a - c) Logarithmic derivatives of the specific heats, C_p/T^3 , with respect to the atomic masses of the constituents, Cu, Ga and S (from top to bottom), respectively. The (black) solid lines represent the logarithmic derivatives calculated from our theoretical heat capacities (ABINIT). (d) (red) \circ Logarithmic derivatives of the specific heat of CuGaS_2 (natural isotope composition) with respect to the temperature. Plotted is the quantity $\frac{1}{2} \times (d \ln C_p / T^3 / d \ln T + 3)$ which is compared with the sum of the logarithmic derivatives with respect to the isotopic masses (blue) \square : experiment; black solid line: sum of theory curves shown in (a - c). At very low temperatures the theoretical logarithmic derivatives have been extrapolated (dashed lines) to the values imposed for $T \rightarrow 0$ by eq. (9-11).

In the case of CuGaS_2 these three ratios are, fortuitously, approximately equal to 0.5.

V. CONCLUSIONS

Ab initio electronic band-structure techniques, especially those which use up-to-date computer codes like VASP or ABINIT, are powerful methods to investigate electronic, optical, vibronic and thermodynamic properties of crystals and the results with experimental data. Here we apply these techniques to CuGaS_2 which has chalcopyrite structure (space group $I\bar{4}2d$ (No. 122), two molecules per primitive cell.) more complicated than those usually dealt with. We used the ABINIT code to calculate the frequencies of Raman and IR phonons and their dispersion relations. The densities of states of one and two phonons have also been calculated. We devote the last section to present experimental data on the specific heat versus temperature of samples grown with the natural isotopic abundances and those grown with isotopically modified ones. These results are compared with *ab initio* calculations. Generally, good agreement between experiment and *ab initio* results is obtained. A redetermination of the crystal structure parameters is presented which decreases the discrepancies with experimental data apparent in the literature. The peaks of the Cu and Ga mass derivatives in Fig. 8 are at similar temperatures. In the process of measuring AgGaS_2 wherein the masses of the two cations are considerably different we observe a clear difference of the low temperature phonon spectrum related to the differences of the atomic masses of Ag and Ga.

Acknowledgments

AHR has been supported by CONACYT Mexico under projects J-83247-F, Binational Collaboration FNRS-Belgium-CONACYT and PPPROALMEX-DAAD-CONACYT. A. M. acknowledges the financial support from the Spanish MCYT under grants MAT2010-21270-C04-03, CSD2007-00045 and the super-computer resources provided by the Red Española de Supercomputación. We are grateful to Y. Pouillon and O. Castillo for valuable technical and computational support. We are also indebted to E. Kotomin for a critical reading of the manuscript.

- * Corresponding author: E-mail R.Kremer@fkf.mpg.de
- ¹ M. Sanati, S. K. Estreicher, and M. Cardona, *Solid State Commun.* **131**, 229 (2004)
 - ² A. Gibin, G.G. Devyatykh, A.V. Gusev, R.K. Kremer, M. Cardona, and H.-J. Pohl, *Sol. State Comm.* **133** 569 (2005).
 - ³ M. Cardona, R. K. Kremer, R. Lauck, G. Siegle, A. Muñoz, and A. H. Romero, and A. Schindler, *Phys. Rev. B* **81** 075207 (2010).
 - ⁴ J.E. Jaffe and A. Zunger, *Phys. Rev. B* **28**, 5822 (1983).
 - ⁵ H. Horinaka, Y. Yamamoto, and T. Miyauchi, *Jap. J. Appl. Phys* **17**, 521 (1978).
 - ⁶ J.Serrano, Ch. Schweitzer, C.T. Lin, K. Reimann, M.Cardona, and D. Fröhlich, *Phys. Rev. B* **65**, 125110 (2002).
 - ⁷ H. Hahn, G. Frank, W. Klingler, A. D. Meyer, G. Stoerger, *Z. Anorg. Allg. Chem.* **271**, 153 (1953).
 - ⁸ H. Strunz, B. H. Geier, E. and Seeliger, *Neues Jahrbuch für Mineralogie, Monatshefte* 241 (1958).
 - ⁹ H. Strunz, B. H. Geier and E. Seliger, *Am. Mineral.* **44**, 906 (1959).
 - ¹⁰ X. Gonze *et al.*, *Comput. Mater. Sci.* **25**, 478 (2002). ABINIT is a collaborative project of the Université Catholique de Louvain, Corning Incorporated and other contributors.
 - ¹¹ X. Gonze, B. Amadon, P.-M. Anglade, J.-M. Beuken, F. Bottin, P. Boulanger, F. Bruneval, D. Caliste, R. Caracas, M. Cote, T. Deutsch, L. Genovese, Ph. Ghosez, M. Giantomassi, S. Goedecker, D. R. Hamann, P. Hermet, F. Jollet, G. Jomard, S. Leroux, M. Mancini, S. Mazevet, M. J. T. Oliveira, G. Onida, Y. Pouillon, T. Rangel, G.-M. Rignanese, D. Sangalli, R. Shaltaf, M. Torrent, M. J. Verstraete, G. Zerah, and J. W. Zwanziger, *Computer Phys. Commun.* **180**, 2582 (2009).
 - ¹² G.Kresse and J. Furthmüller, *Comp. Mat Sci* **6**, 15 (1996).
 - ¹³ G.Kresse, D. K. Joubert, *Phys Rev. B* **59**, 1758 (1999) and references therein.
 - ¹⁴ M. Fuchs, M. Scheffler, *Comput. Phys. Commun.* **119**, 67 (1999).
 - ¹⁵ M. Cardona, R. K. Kremer, G. Siegle, A. Muñoz, A. H. Romero, and M. Schmidt, *Phys. Rev B* **82**, 085210 (2010).
 - ¹⁶ R. W. Godby, M. Schlüter, and L. J. Sham, *Phys. Rev B* **37**, 10159 (1988).
 - ¹⁷ A. Shileika, *Surf. Science* **37**, 730 (1973).
 - ¹⁸ A. Soni, V. Gupta, C. M. Arora, A. Dashora and B. L. Ahuja, *Solar Energy* **84**, 1481 (2010).
 - ¹⁹ M. G. Brik, *J. Phys.: Condens. Matter* **21**, 485502 (2009).
 - ²⁰ B.Tell and P.M. Bridengaugh, *Phys Rev. B* **12**, 3330 (1975).
 - ²¹ K. Shindo, A. Morita, and H. Kamimura, *J. Phys. Soc. Japan* **20**, 2054 (1945).
 - ²² P. Carrier and Su-Huai Wei, *Phys. Rev. B* **70**, 035212 (2004)
 - ²³ M. Cardona, R. K. Kremer, R. Lauck, G. Siegle, A. Muñoz, and A. H. Romero, *Phys. Rev. B* **80**, 195204 (2009).
 - ²⁴ X. Gonze, *Phys. Rev. B* **55**, 10337 (1997).
 - ²⁵ X. Gonze and C. Lee, *Phys. Rev. B* **55**, 10355 (1997).
 - ²⁶ Further information about data collection, data reduction, refinement and geometrical details can be obtained from Fachinformationszentrum Karlsruhe, D-76344 Eggenstein-Leopoldshafen (Fax: +49-7247-808-666, e-mail: crysdata@fiz-karlsruhe.de) by quoting the deposition number CSD-422615.
 - ²⁷ NETZSCH-Gerätebau GmbH, Wittelsbacherstr. 42, D-95100 Selb, Germany.
 - ²⁸ J. Serrano, R. K. Kremer, M. Cardona, G. Siegle, A. H. Romero, and R. Lauck, *Phys. Rev. B* **73**, 094303 (2006).
 - ²⁹ J. E Jaffe and A. Zunger, *Phys. Rev.* **28**, 5822 (1983).
 - ³⁰ Shiyong Chen, X. G. Gong, and Su-Huai Wei, *Phys. Rev B* **75**, 205209 (2007).
 - ³¹ D. R. Hamann, X. Wu, K. M. Rabe, and D. Vanderbilt, *Phys. Rev. B* **71**, 035117 (2005).
 - ³² C. Parlak and R. Eryigit, *Phys. Rev. B* **73**, 245217 (2006).
 - ³³ Hou Hai-Jun, Zhu Shi-Fu, Zhao Bei-Jun, Yu You, and Xie Lin-Hua, *Phys. Scr.* **82**, 055601 (2010).
 - ³⁴ M. Bettini and W. B. Holzapfel, *Solid State Commun.*, **16**, 27 (1975).
 - ³⁵ A. Werner, H. D. Hochheimer, and A. Jayaraman, *Phys. Rev. B* **23**, 3836 (1981).
 - ³⁶ T. Tinoco, J.P. Itié, A. Polian, A. San Miguel, E. Moya, P. Grima, J. Gonzalez, and F. Gonzalez, *J. Physique IV C* **9**, 151 (1994).
 - ³⁷ C. Carlone, D. Olego, A. Jayaraman, and M. Cardona, *Phys. Rev.* **22**, 3877 (1980).
 - ³⁸ M. Akdoğan and R. R. Eryigit, *J. Phys.: Condens. Matter* **14**, 7493 (2002).
 - ³⁹ J. Serrano, A. H. Romero, F. J. Manjón, R. Lauck, M. Cardona, and A. Rubio, *Phys. Rev B* **69**, 094306 (2004).
 - ⁴⁰ J. Serrano, A. Cantarero, M. Cardona, N. Garro, R. Lauck, R. E. Tallman, T. M. Ritter, and B. A. Weinstein, *Phys. Rev. B* **69**, 014301 (2004).
 - ⁴¹ M. Cardona and M. L. W. Thewald, *Rev. Mod. Phys.* **77**, 1173 (2005).
 - ⁴² A. Debernardi and M. Cardona, *Phys. Rev. B* **54**, 11305 (1996).
 - ⁴³ I. V. Bodnar and N. S. Orlova, *phys. stat. sol. (a)* **78**, K59 (1983).
 - ⁴⁴ S. Schorr and D. Sheptyakov, *J. Phys.: Cond. Matter* **20** 104245 (2008).
 - ⁴⁵ N. Yamamoto, H. Horinaka, and T. Miyauchi, *Jap. J. Appl. Phys.* **18**, 255 (1979).
 - ⁴⁶ A. U. Malsagov, I. M. Berfirer, and B. S. Kulbezhev, *Izv. Vyssh. Ucheb. Zav., Fizika* **29**, 126 (1986); cited from H. Neumann, *Cryst. Res. Technol.* **22**, 723 (1987).
 - ⁴⁷ R. R. Reeber and G. W. Powell, *J. Appl. Phys.*, **38**, 1531 (1967); R. R. Reeber, *phys. stat. solidi a* **32**, 321 (1975).
 - ⁴⁸ R. B. Roberts, G. K. White, and T. M. Sabine, *Aust. J. Phys.* **34**, 701 (1981).
 - ⁴⁹ S. Q. Wang, *Appl. Phys. Lett.* **88**, 061902 (2006).
 - ⁵⁰ S. C. Abrahams and F. S. L.Hsu *J. Chem. Phys.* **63**, 1162 (1975).
 - ⁵¹ H. Neumann, G. Kühn, and W. Möller, *phys. stat. solidi B* **144**, 565 (1987).
 - ⁵² A. H. Romero, M. Cardona, R. K. Kremer, R. Lauck, G. Siegle, J. Serrano, and X. C. Gonze, *Phys. Rev. B* **78**, 224302 (2008).
 - ⁵³ M. Cardona, R. K. Kremer, R. Lauck, G. Siegle, J. Serrano, and A. H. Romero, *Phys. Rev. B* **76**, 075211 (2007).